Titan airglow during eclipse

R. A. West,[1] J. M. Ajello,[1] M. H. Stevens,[2] D. F. Strobel,[3] G. R. Gladstone,[4] J. S. Evans,[5] and E. T. Bradley[6]

Received 30 July 2012; revised 20 August 2012; accepted 23 August 2012; published 28 September 2012.

[1] Solar XUV photons can provide enough energy to account for the observed nitrogen UV dayglow emissions above 800 km, but a small or sporadic contribution from energetic particles cannot be ruled out. Furthermore, ion production at altitudes deeper than 800 km as inferred from radio occultation cannot be produced by solar XUV stimulation and implies energy deposition from protons and oxygen ions. Here we examine UV spectra and visible-wavelength images of Titan in Saturn's shadow, when XUV stimulation is absent. UV emissions are observed in one of the three sets of spectra, and the intensity of these emissions is about a factor of 10 less than the peak intensity reported on the dayside. We observe visible-wavelength emissions for the first time. No horizontally resolved auroral structures are seen in the visible images. At visible wavelengths Titan has a global emission at the haze-top level that is not understood, although cosmic ray ionization and chemiluminescence are candidates needing further investigation. **Citation:** West, R. A., J. M. Ajello, M. H. Stevens, D. F. Strobel, G. R. Gladstone, J. S. Evans, and E. T. Bradley (2012), Titan airglow during eclipse, *Geophys. Res. Lett.*, *39*, L18204, doi:10.1029/2012GL053230.

1. Introduction

[2] For Titan, one of the most difficult problems is to estimate the role that precipitating energetic particles (electrons, protons, oxygen ions and cosmic rays) play in producing Titan's airglow and chemistry, and in contributing to the energetics of the atmosphere [*Cravens et al.*, 2009; *Sittler et al.*, 2009]. Ionization on the dayside and terminator region by solar XUV photons makes such a determination extremely difficult. To date, only upper limits have been put on dark side emissions [*Hall et al.*, 1992].

[3] During 2009, Titan passed through Saturn's shadow, offering a unique opportunity to observe airglow emission from Titan in the absence of solar XUV stimulus. Observations by the Imaging Science Subsystem (ISS) and the Ultraviolet Imaging Spectrograph (UVIS) provide a sensitive measure of airglow stimulated by energetic charged particles. Here we present the first airglow observations of Titan when it is free from solar XUV excitation.

2. Observations and Analysis

[4] Images from ISS and spectra from UVIS were obtained on three occasions (two in 2009 and one in 2010). The first, on day 127 of 2009 was the most favorable because the spacecraft distance was smallest (644030.8–677599.8 km) and Titan was most deeply immersed in Saturn's shadow (radial distance from the center line was 0.45–0.75 of Saturn's radius). The remainder of this paper concerns only this event.

[5] The sub-solar latitude and longitude were near 0° and 360°, respectively and the sub-spacecraft latitude and longitude were −53.6° and 328.5° on day 127 of 2009. The spacecraft was off the dusk side of Saturn looking at the side of Titan facing the ram (upstream) direction of Saturn's co-rotating plasma. The positions of the spacecraft and Titan can be seen in Figure S1 in the auxiliary material.[1] The UVIS spatial pixel scale was of 650 km/pixel, too large to provide meaningful vertical profiles (see Figure S2). The ISS Wide Angle Camera (WAC) image scale is 40 km/pixel.

2.1. Spectral Analysis of UVIS Eclipse Data

[6] We assembled and averaged 57 spectra from 8:27:34 to 10:50:14 UT on May 7 2009 and from all pixels with tangent heights of 0–2000 km. Analogous to the approach of *Stevens et al.* [2011] we synthesize four different sets of emissions: the bright H Lyman-α feature near 1216 Å, the N_2 Lyman-Birge-Hopfield (LBH) $a^1\Pi_g$—^1X_g system, the N_2 Vegard-Kaplan (VK) $A^3\Sigma_u^+ - X^1\Sigma_g^+$ system and N I multiplets. Because the signal/noise ratio of the nitrogen data is low, this study assumed relative intensities of the emission features within these sets of emissions are the same as the solar driven features used by *Stevens et al.* [2011]. This assumption could be relaxed for data with sufficiently high signal/noise and knowledge of the energy spectrum of precipitating particles. We use a methane slant column of 2.4×10^{16} cm^{-2} in all of our spectral fits, consistent with that used for the dayglow observations of *Stevens et al.* [2011] at 1000 km tangent altitude. The emissions are smoothed with the UVIS spectral resolution function that is constrained by separate dayglow observations of the bright N I 1493 Å feature. The four vectors are used in a least-squares regression fit to the observation and the results for the nitrogen emissions are indicated in Figure 1, with retrieved limb radiances from fitting the spectra indicated. To produce this figure we removed a constant background from the FUV

[1]Jet Propulsion Laboratory, California Institute of Technology, Pasadena, California, USA.
[2]Space Science Division, Naval Research Laboratory, Washington, D. C., USA.
[3]Department of Earth and Planetary Sciences, Johns Hopkins University, Baltimore, Maryland, USA.
[4]Space Science and Engineering, Southwest Research Institute, San Antonio, Texas, USA.
[5]Computational Physics Inc., Springfield, Virginia, USA.
[6]Department of Physics, University of Central Florida, Orlando, Florida, USA.

Corresponding author: R. A. West, Jet Propulsion Laboratory, California Institute of Technology, MS 183-501, 4800 Oak Grove Dr., Pasadena, CA 91109, USA. (robert.a.west@jpl.nasa.gov)

0094-8276/12/2012GL053230

[1]Auxiliary materials are available in the HTML. doi:10.1029/2012GL053230.

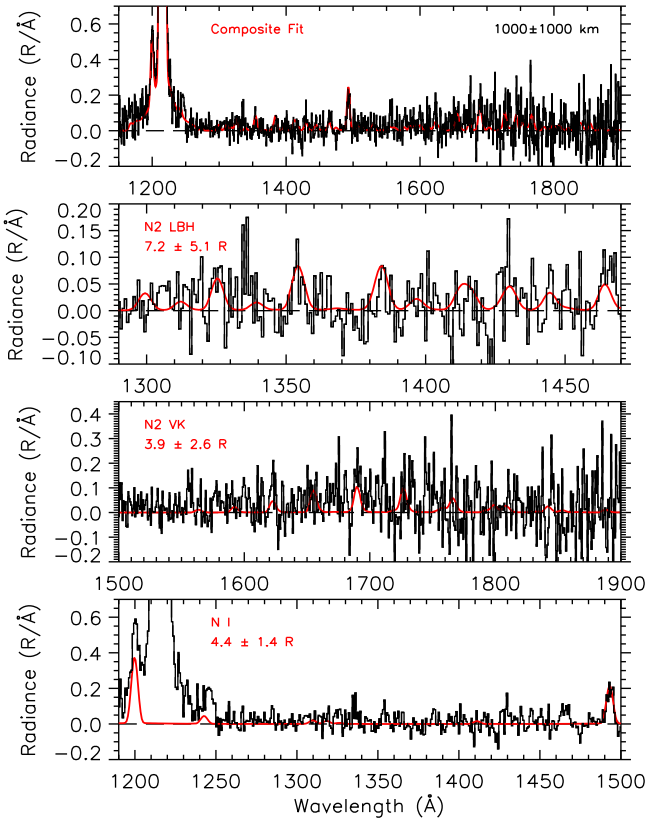

Figure 1. (top) UVIS Titan FUV airglow data on 7 May 2009 between 8:27 and 10:50 UT while in Saturn's shadow. The composite fit to the data is overplotted in red and the altitudes over which the data is averaged are indicated. (top middle) Same as Figure 1 (top) but showing the component of the fit from the N_2 LBH bands Radiances and uncertainties from the fit over the wavelength region in Figure 1 (top) are indicated. (bottom middle) Same as Figure 1 (top middle) but showing the component of the fit from the N_2 VK bands instead. (bottom) Same as Figure 1 (top middle) but only showing the component of the fit from the N I features.

data that is of the order 0.03 R/Å, most likely due to an unknown broadband emission source.

[7] Figure 1 (top) shows the data with the composite fit over-plotted. The three separate contributions from processes involving N_2 to the composite fit are split out in the three panels below. Radiances and uncertainties in Figures 1 (top middle), 1 (bottom middle), and 1 (bottom) are calculated over the entire fitted wavelength region, although the spectral region in each panel is limited to where each set of emissions is brightest. Figure 1 (top middle) shows the contributions of the N_2 LBH bands. The N_2 LBH radiance is about a factor of 15 less than the peak LBH limb radiance reported from dayglow observations [*Stevens et al.*, 2011]. It should be emphasized that the vertical resolution of the dayglow observations was about a factor of ten higher than the limb observations presented here. Figure 1 (bottom middle) shows the contribution due to the N_2 VK bands with the radiance and uncertainty also indicated. Although the VK (7,0) band is discernable near 1689 Å, the total VK emission indicated is also about a factor of 15 weaker than the peak dayglow radiance reported by *Stevens et al.* [2011]. Figure 1 (bottom) shows the contribution due to N I emission, which is dominated by the N I 1200 Å and N I 1493 Å multiplets and where the total N I emission is about a factor of 6 less than the reported dayglow radiance.

[8] The airglow signal in the UVIS EUV channel is weak so we limit our EUV analysis to wavelengths between 1000–1100 Å where the brightest features are identifiable. In Figure 2 we use the same approach as for the FUV, synthesizing the predominant features at high resolution and then smoothing the spectrum with the UVIS spectral resolution function. We limit the analysis to three EUV features or systems: the H Ly-β feature at 1026 Å, the N II 1085 Å multiplet and the other weaker N I features. We use the same column abundance of methane as we did with the FUV (2.4×10^{16} cm^{-2}). The contributions from H Ly β (0.5 ± 0.1 R) and N II 1085 Å (0.4 ± 0.1 R) are indicated with their associated fitting uncertainties. The N II 1085 Å multiplet is about a factor of ten weaker than reported from the dayglow observations [see *Stevens et al.*, 2011].

2.2. The ISS Observations and Interpretation

[9] Twenty four WAC images were obtained using exposure times from 10 s to 560 s in broad-band filters from near-UV (315 nm) to near-IR (1000 nm), including the clear filters covering the entire spectral range of the cameras [see *Porco et al.*, 2004]. We have images from the Narrow Angle Camera as well, but only the WAC (which has the faster optical system) shows an airglow signal, with highest signal/noise ratio in the [CL1,CL2] filter combination sensitive to light from the violet (~4000 Å) to near infrared (~11000 Å). Figure 3 shows one of the images (frame W1620383876).

[10] Three sources of illumination are evident in Figure 3. In Figure 3a light refracted and scattered by Saturn's high atmosphere and by the rings illuminates the bottom portion of the disk, producing I/F $< 4 \times 10^{-6}$, where I is the intensity and πF is the solar flux at Titan. That is a factor of 2×10^{-5} weaker than Titan in direct sunlight at the same phase angle. In Figure 3b that component has been subtracted using a similarly-illuminated image in sunlight and what remains are two components: Titan's optically thick haze below 300 km altitude illuminated by unknown sources (I/F ~ 10^{-7}), and a very faint glow on the limb (I/F ~ 2×10^{-8}) in the optically thin region between 300 km altitude (the inner dashed circle) and 1000 km (the outer dashed circle).

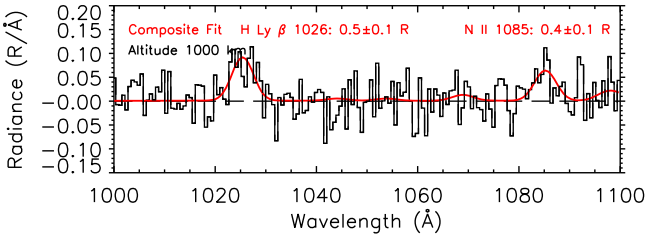

Figure 2. UVIS Titan EUV airglow data while in Saturn's shadow. The composite fit to the data is overplotted in red and the altitudes over which the data is averaged are the same as in Figure 1. The H Ly β and N II 1085 Å radiance is indicated with the fitted uncertainty.

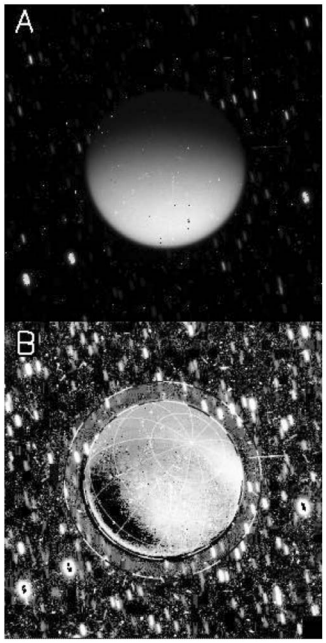

Figure 3. Two views of image W1620383876, a 560 s exposure in the [CL1,CL2] (clear) filter combination. (a) Brightness is proportional to intensity, with maximum I/F = 4×10^{-6}. The direction to Saturn is downward. Background star trails and cosmic ray events are apparent. (b) Light from Saturn's limb and rings has been subtracted by using an image in sunlight at nearly the same phase angle, and intensity scaled to maximum I/F = 2×10^{-7}. A latitude/longitude grid has been placed on the image showing the location of the south pole. The dashed circles in Figure 4b are located at 300 km and 1000 km altitude.

[11] We examined the possibility that Hyperion, Iapetus and Phoebe might be sources of illumination for Titan's anti-sun hemisphere. The sub-Titan meridians of Hyperion and Iapetus are about 90 degrees or more from the Cassini meridian. They would produce a crescent of illumination on the right side of Titan in Figure 3b, leaving the left side in shadow. That is not what is seen. The part of Titan's disk beyond the terminator (from Saturn shine) is left/right symmetric. The asymmetric portion of the disk is less reliable because a relatively large component was subtracted and the small residual is subject to error (such as a centering error or latitudinal gradients in the subtracted image not matching those in the eclipse image). Phoebe-shine is too weak by four orders of magnitude.

[12] Internal sources of illumination must also be evaluated for the source of light at the haze level. Cosmic rays penetrate to deep levels. Ionization and subsequent airglow emission from that process may contribute. Lightning is not a candidate [see *Fischer and Gurnett*, 2011]. Chemiluminescence from a long-lived excited state produced on the dayside and advected to the night side is a possibility. For example, Titan's ionosphere is dominated by HCNH+, which is a terminal ion. Assuming an ionosphere density of 1000 cm^{-3} at an electron temperature of 1000 K over an altitude range of 1000 km [cf. *Cravens et al.*, 2009], the electron recombination reaction $HCNH^+ + e \rightarrow CN + H_2$ could yield ~13 R of near-UV to visible CN emissions (assuming a recombination rate of 2.8E-7(300/T)$^{0.65}$ and a yield of 33% for this path [*Semaniak et al.*, 2001]). Finally, emissions produced by energetic protons or oxygen ions precipitating from Saturn's magnetosphere may be responsible for the much weaker intensity in the optically thin region above 600 km. They are not expected to be significant sources below 300 km [*Cravens et al.*, 2008, 2009].

[13] The weak signal between 300 and 1000 km altitude is very close to the noise level. The signal persists in deconvolved images, allowing us to rule out as its origin a convolution of the camera point spread function (PSF) with the brighter part of the disk. The signal is nearly uniform with location around the limb (about equal beyond the terminator as on the sun-facing side), unlike what would be produced by a convolution of the asymmetric solar illumination with the camera PSF. The signal is nearly uniform with altitude between 300 and 1000 km altitude. Magnetospheric electrons do not penetrate below about 800 km and so the energy source may be precipitating protons or oxygen ions [*Cravens et al.*, 2008, 2009].

[14] A faint limb signal similar to that shown in Figure 3b is seen in ISS broadband filter images from blue (central wavelength 4510 Å) to IR2 (8620 Å). Emissions were not detected in the WAC violet filter (4200 Å) or the IR3 filter (9300 Å). We had hoped to compare filter observations with the predictions for electron impact [*Mangina et al.*, 2011] but the signal/noise ratio of the observations was not sufficiently high for that purpose.

3. Hydrogen Emissions

[15] Although Titan experiences no direct EUV solar illumination while in Saturn's shadow, interstellar H atoms redirect the Sun's flux of Lyα photons via resonance scattering to produce a roughly uniform glow of interplanetary (IPM) Lyα emission. During the eclipse observations, UVIS observed Titan with the upstream (λ = 252°, β = 8.9° [*Lallement et al.*, 2010]) IPM in the background, so that the sub-Cassini point on the eclipsed disk of Titan was illuminated by the downstream hemisphere of the sky. We model the scattering of IPM Lyα in Titan's atmosphere (P. Hedelt, private communication, 2011) using the resonance line radiative transfer code of *Gladstone et al.* [2004]. Based on models [*Pryor et al.*, 2012] we take the IPM Lyα source present at Titan to be uniform at 250 R brightness, with a Gaussian line profile appropriate for an IPM H temperature of 12,000 K [*Izmodenov*, 2009], with a Doppler redshift of 22·cos(zenith angle) [in km/s]. We approximate the IPM illumination in 10°-wide zenith angle annuli, and sum the results to obtain the total emission rate. Details are shown in Figure S3.

[16] The model predicts ~23 R of Lyα emission from the sub-Cassini region of Titan. This is roughly half of what is observed in the UVIS spectrum. The observations show 41.9 ± 1.6 R of emergent Ly α emission from Titan's disk during these observations. The remaining 19 R may be produced by charge exchange with impacting protons, a strong excitation process of Lyα observed in the laboratory [*Ajello et al.*, 2011] with a small contribution from the IPM along the line of sight from the spacecraft to Titan. This residual 19 R emission source is most probably due to precipitating protons because according to *Strickland et al.* [1993] the yield of Lyα to total LBH photons in terrestrial proton auroras

is ~1–2, depending on incident proton energies and after cross section adjustments discussed in *Correira et al.* [2011]. From the observed intensity of the detected LBH bands in Figure 1 (top) (7.2 ± 5.1 R), we would therefore expect the emergent Lyα intensity to be 25–50 R due to both an interplanetary contribution and proton excitation. We know that both H and O ions are present in Saturn's magnetosphere [e.g., *Cravens et al.*, 2008] and this would permit an admixture of precipitating protons and O^+ ions. Magnetospheric electron production of Lyα by H_2 dissociative excitation would be negligible because most of the electron energy would be deposited below the exobase where H_2 is a minor constituent, as is H.

4. Discussion

[17] One of the important scientific objectives of the Cassini Mission is to determine the relative contributions of magnetospheric energy and solar energy inputs to Titan's upper atmosphere. From the FUV airglow measurements in eclipse reported here with intensities an order of magnitude lower than in the FUV dayglow, the direct inference would be that solar input is approximately a factor of ten more important than magnetospheric input. The fact that both the N II 1085 Å and the N I multiplets are about a factor of six to ten weaker than in the dayglow [*Stevens et al.*, 2011] implies that most magnetospheric FUV emission is produced above the CH_4 $\tau = 1$ level or ~850 km. According to *Cravens et al.* [2008] lower energy (<30 keV) oxygen ions and protons would deposit most of their energy above this level.

[18] With better S/N and detailed model plasma calculations beyond the scope of this letter, diagnosing the nature of the precipitating particles and their energy spectrum from the airglow of Titan would allow us to quantify the interaction between Saturn's magnetosphere and Titan's upper atmosphere. Simulating the relative intensity of the observed emission features with a model that contains all the relevant excitation processes by electrons, protons and O^+ is the means by which this can be done. Although the N_2 LBH and VK bands are the two brightest systems in Titan's UV airglow, the relative intensities of the individual emission features are subject to uncertainties in yields from electron, proton and ion impact as well as uncertainties in cascade contributions to N_2 LBH and VK bands from higher lying states [*Eastes*, 2000; *Ajello et al.*, 2010; *Correira et al.*, 2011; *Stevens et al.*, 2011; *Bhardwaj and Jain*, 2012]. The most useful diagnostics for deriving the incident energy spectrum are the features arising directly from electron, proton and ion impact with N and/or N_2 (e.g., N II 1085 Å and N I 1493 Å), which are not subject to cascade contributions. Additionally, valuable new insight can be gained through limb observations with higher vertical resolution over the extensive ionosphere from 500–1400 km than what is shown here to locate the peak altitude of the precipitating particles and thereby constrain their characteristic energy. Unfortunately methane absorption blocks emission below 800 km except for strong features above 1400 Å wavelength indicating a high S/N observation of 1493 Å, is an ideal candidate. The distant FUV eclipse data reported indicate the magnetosphere energy input to be a minor source (~10%) of globally averaged energy input to Titan's upper atmosphere.

[19] **Acknowledgments.** We thank Pascal Hedelt who supplied tables of H and CH_4 densities in Titan's atmosphere. DFS was supported by the Cassini-Huygens Mission through JPL contract 109303. JMA and MHS were supported by the NASA Cassini Data Analysis Program and Planetary Atmospheres Program. RAW was supported by the Cassini-Huygens mission and by the NASA Astrobiology Institute. Part of this work was performed by the Jet Propulsion Laboratory, California Institute of Technology, under a contract with the National Aeronautics and Space Administration.

[20] The Editor thanks Anil Bhardwaj and an anonymous reviewer for assisting in the evaluation of this paper.

References

Ajello, J. M., R. S. Mangina, and R. R. Meier (2010), UV molecular spectroscopy from electron-impact for applications to planetary atmospheres and astrophysics, in *Charged Particle and Photon Interactions With Matter: Recent Advances, Applications, and Interfaces*, edited by Y. Hatano et al., chap. 28, pp. 761–804, Taylor and Francis, Boca Raton, Fla., doi:10.1201/b10389-29.

Ajello, J. M., R. S. Mangina, D. J. Strickland, and D. Dziczek (2011), Laboratory studies of UV emissions from proton impact on N_2: The Lyman-Birge-Hopfield band system for aurora analysis, *J. Geophys. Res.*, *116*, A00K03, doi:10.1029/2010JA016103.

Bhardwaj, A., and S. K. Jain (2012), Production of N_2 Vegard-Kaplan and other triplet band emissions in the dayglow of Titan, *Icarus*, *218*, 989–1005, doi:10.1016/j.icarus.2012.01.019.

Correira, J., D. J. Strickland, J. S. Evans, H. K. Knight, and J. H. Hecht (2011), A downward revision of a recently reported proton auroral LBH emission efficiency, *J. Geophys. Res.*, *116*, A07303, doi:10.1029/2010JA016016.

Cravens, T. E., I. P. Robertson, S. A. Ledvina, D. Mitchell, S. M. Krimigis, and J. H. Waite Jr. (2008), Energetic ion precipitation at Titan, *Geophys. Res. Lett.*, *35*, L03103, doi:10.1029/2007GL032451.

Cravens, T. E., R. V. Yelle, J.-E. Wahland, D. E. Shemansky, and A. F. Nagy (2009), Composition and structure of the ionosphere and thermosphere, in *Titan From Cassini Huygens*, edited by R. H. Brown, J.-P. Lebreton, and J. H. Waite, chap. 11, pp. 259–295, Springer, Heidelberg, Germany, doi:10.1007/978-1-4020-9215-2_11.

Eastes, R. W. (2000), Modeling the N_2 Lyman-Birge-Hopfield bands in the dayglow: Including radiative and collisional cascading between the singlet states, *J. Geophys. Res.*, *105*(A8), 18,557–18,573, doi:10.1029/1999JA000378.

Fischer, G., and D. A. Gurnett (2011), The search for Titan lightning radio emissions, *Geophys. Res. Lett.*, *38*, L08206, doi:10.1029/2011GL047316.

Gladstone, G. R., W. R. Pryor, W. K. Tobiska, A. I. F. Stewart, K. E. Simmons, and J. M. Ajello (2004), Constraints on Jupiter's hydrogen corona from Galileo UVS observations, *Planet. Space Sci.*, *52*, 415–421, doi:10.1016/j.pss.2003.06.012.

Hall, D. T., D. E. Shemansky, and T. M. Tripp (1992), A reanalysis of Voyager UVS observations of Titan, in *Symposium on Titan, Eur. Space Agency Spec. Publ., ESA*, *SP-338*, 69–74.

Izmodenov, V. V. (2009), Local interstellar parameters as they are inferred from analysis of observations inside the heliosphere, *Space Sci. Rev.*, *143*, 139–150, doi:10.1007/s11214-008-9444-y.

Lallement, R., E. Quemerais, D. Koutroumpa, J.-L. Bertaux, S. Ferron, W. Schmidt, and P. Lamy (2010), The interstellar H flow: Updated analysis of SOHO/SWAN data, in *Twelfth International Solar Wind Conference, AIP Conf. Proc.*, *121*, 555–558, doi:10.1063/1.3395925.

Mangina, R. S., J. M. Ajello, R. A. West, and D. Dziczek (2011), High-resolution electron-impact emission spectra and vibrational emission cross sections from 330–1100 nm for N_2, *Astrophys. J. Suppl. Ser*, *196*, 13, doi:10.1088/0067-0049/196/1/13.

Porco, C., et al. (2004), Cassini imaging science: Instrument characteristics and anticipated scientific investigations at Saturn, *Space Sci. Rev.*, *115*, 363–497, doi:10.1007/s11214-004-1456-7.

Pryor, W. R., G. M. Holsclaw, W. E. McClintock, M. A. Snow, R. J. Vervack Jr., G. R. Gladstone, S. Alan Stern, K. D. Retherford, and P. Miles (2012) Lyman-alpha Models for LRO LAMP from MESSENGER MASCS and SOHO SWAN data, in *Cross-Calibration of Past and Present Far UV Spectra of Solar System Objects and the Heliosphere*, *ISSI Sci. Rep.*, vol. 12, edited by E. Quemerais, M. Snow, and R. M. Bonnet, in press.

Semaniak, J., B. F. Minaev, A. M. Derkatch, F. Hellberg, A. Neau, S. Rosén, R. Thomas, and M. Larsson (2001), Dissociative recombination of $HCNH^+$: Absolute cross-sections and branching ratios, *Astrophys. J. Suppl. Ser.*, *135*, 275–283, doi:10.1086/321797.

Sittler, E. C., R. E. Hartle, C. Bertucci, A. Coates, T. Cravens, I. Dandouras, and D. Shemansky (2009), Energy deposition processes in Titan's upper atmosphere and its induced magnetosphere, in *Titan From Cassini Huygens*, edited by R. H. Brown, J.-P. Lebreton, and J. H. Waite, chap. 16, pp. 393–453, Springer, Heidelberg, Germany, doi:10.1007/978-1-4020-9215-2_16.

Stevens, M. H., et al. (2011), The production of Titan's ultraviolet nitrogen airglow, *J. Geophys. Res.*, *116*, A05304, doi:10.1029/2010JA016284.

Strickland, D. J., R. Daniell, J. Jasperse, and B. Basu (1993), Transport-theoretic model for the electron-proton-hydrogen atom aurora: 2. Model results, *J. Geophys. Res.*, *98*(A12), 21,533–21,548, doi:10.1029/93JA01645.